Rotor Fault Detection and Identification for a Hexacopter Based on Control and State Signals via Statistical Learning Methods

Airin Dutta PhD Student
Michael McKay PhD Student
Fotis Kopsaftopoulos Assistant Professor
Farhan Gandhi Redfern Professor Director

Center for Mobility with Vertical Lift (MOVE)
Rensselaer Polytechnic Institute, Troy, NY

ABSTRACT

A robust framework for fault detection and identification of rotor degradation in multicopters while effectively rejecting the effects of gusts is introduced. The rotor fault detection and identification methods employed in this study are based on excitation-response signals of the aircraft under ambient turbulence to distinguish between an aircraft response to gusts and rotor faults. A concise overview of the development of statistical time series model for healthy aircraft using the aircraft attitudes as the output and controller commands as the input is presented. This model is utilized to extract quality features for training a simple neural network to perform effective online rotor fault detection and identification in a hexacopter exceptional speed of making a decision and accuracy of fault classification. It is shown that using a statistical time series model assisted neural network employed for online monitoring is capable of rejecting gusts, sensitive to even 20% rotor degradation and achieves fault detection and identification in less than 2 s after the fault with an accuracy over 99%.

NOTATION

α	:	Type I risk level
β	:	Type II risk level
γ	:	Autocorrelation
τ	:	Lag
σ^2	:	Residual variance
Σ	:	Residual covariance matrix
ARX	:	AutoRegressive with eXogenous excitation
BIC	:	Bayesian Information Criterion
CCF	:	Cross-Covariance Function
$E\{\cdot\}$	:	Expected value
FDI	:	Fault Detection and Identification
iid	:	identically independently distributed
LS	:	Least Squares
PE	:	Prediction Error
PSD	:	Power Spectral Density
RSS	:	Residual Sum of Squares
SPP	:	Samples Per Parameter
SPRT	:	Sequential Probability Ratio Test
SSS	:	Signal Sum of Squares
UCL	:	Upper Control Limit
LCL	:	Lower Control Limit
VAR	:	Vector AutoRegressive

Presented at the VFS International 76th Annual Forum & Technology Display, Virginia Beach, Virginia, USA, October 6–8, 2020.

INTRODUCTION

Multicopters, being capable of hovering and vertical take-off and landing, have attracted the interest of the community with respect to both commercial and defense applications over the last decade. Given the increasing interest and widespread use of these vehicles in a number of important arenas such as Urban air Mobility (UAM), early fault detection and identification (FDI) of such systems are critical in order to ensure and improve their overall safety and reliability. Rotorcraft are complex systems that exhibit strong dynamic coupling between rotors, fuselage, and control inputs, as well as time-varying and cyclo-stationary behavior. As a result, they face certain system modeling and fault detection and identification challenges that are not present in fixed-wing aircraft. These issues, as well as potential solutions, have been explored in the recent literature.

An algorithm for online detection of motor failure using only inertial measurements and control allocation by an exact redistributed pseudo-inverse method for octacopters has been demonstrated by Frangenberg et al. (Ref. 1). Heredia and Ollero (Ref. 2) have addressed sensor fault identification in small autonomous helicopters using Observer/Kalman Filter identification. Fault tolerant control for multi-rotors (Refs. 3–6), as well as various fault diagnosis methods such as analytical models, signal processing, and knowledge-based approaches for helicopters have also been proposed (Ref. 7).

A hybrid FDI algorithm comprising of a bank of continuous-time residual generators and a discrete-event system (DES) fault diagnoser have been developed in Ref. 8 to distinguish the effects of disturbances such as gusts from faults without compromising the detection of incipient faults for a network of unmanned vehicles. An actuator fault-tolerant controller with active disturbance rejection based on an extended state observer and nonlinear compensation able to reject gusts and measurement noises has been developed for attitude control of quadcopters (Ref. 9).

Statistical time series methods have been used to detect actuator, control surface, and sensor faults in aircraft systems due to their simplicity, efficient handling of uncertainties, no requirement of physics based knowledge, and applicability to different operating conditions (Refs. 10–13). Dimogianopoulos et al. (Ref. 14) have demonstrated the effectiveness of two statistical schemes based on Pooled Non-Linear AutoRegressive Moving Average with eXogenous excitation (P-NARMAX) representations to detect and isolate faults for aircraft systems under different flight conditions, turbulence levels, and fault types and magnitudes. The first method models the pilot input and aircraft pitch rate relationship, while the second approach models the relationship between horizontal and vertical acceleration, angle of attack and pitch rate signals in fixed-wing aircraft.

Fast and accurate rotor failure detection and identification by various data-driven and statistical learning methods for forward flight under different levels of turbulence using aircraft state signals only has been achieved in 15–17. But, it has been observed that false alarms have increased to a maximum of 30% under presence of gusts with the statistical and knowledge-based methods (Ref. 15). Time-series assisted neural networks described in 16 have shown no false alarms under gusts, which may be attributed to the fact that it has been trained to raise alarms only under complete rotor failures which have a considerable transient response compared to response due to gusts. Hence, this current study aims at expanding the scope of faults to include incipient faults and use the corroboration between control signals and output signals to differentiate between rotor degradation and aircraft response to gusts that may oftentimes mimic the effects of faults on the vehicle dynamics.

APPROACH

Physics-Based Modeling of Multicopter System

A flight simulation model has been developed for a regular hexacopter (Fig. 1) using summation of forces and moments to calculate aircraft accelerations. This model is the source of simulated data under varying operating and

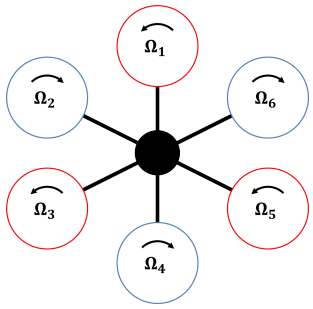

Figure 1: Schematic representation of a regular hexacopter

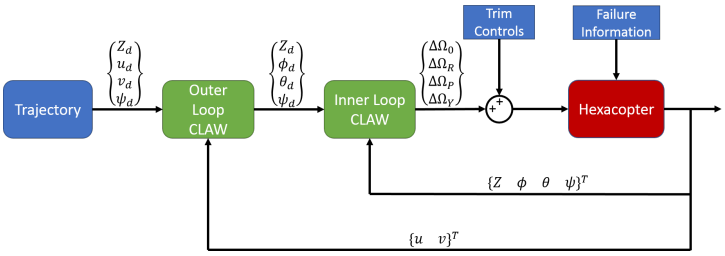

Figure 2: Controller Block Diagram

environmental conditions, as well as different fault types. Rotor loads are calculated using Blade Element Theory coupled with a 3×4 Peters-He finite state dynamic wake model (Ref. 18). This model allows for the simulation of abrupt rotor failure by ignoring the failed rotor inflow states and setting the output rotor forces and moments to zero.

A feedback controller is implemented on the nonlinear model to stabilize the aircraft altitude and attitudes, as well as track desired trajectories written in terms of the aircraft velocities. This controller is designed at multiple trim points, with gain scheduling between these points to improve performance throughout the flight envelope.

The state vector consists of the 12 rigid body states and is defined in Eq. 1.

$$\mathbf{x} = \begin{Bmatrix} X & Y & Z & \phi & \theta & \psi & u & v & w & p & q & r \end{Bmatrix}^T \tag{1}$$

The input vector is comprised of the first four independent multirotor controls for collective, roll, pitch and yaw and is defined in Eq. 2:

$$\mathbf{u} = \begin{Bmatrix} \Omega_0 & \Omega_R & \Omega_P & \Omega_Y \end{Bmatrix}^T \tag{2}$$

The control architecture is illustrated in Fig. 2 and detailed in Ref. 3. This control design has been demonstrated to perform well even in the event of rotor 1,2 or 6 failure, with no adaptation in the control laws themselves.

Data Generation

A continuous Dryden wind turbulence model (Ref. 19) has been implemented in the flight simulation model. The Dryden model is dependent on altitude, length scale, and turbulence intensity and outputs the linear and angular velocity components of continuous turbulence as spatially varying stochastic signals. The proper combination of these parameters determines the fit of the signals to observed turbulence.

In this system, altitude is taken as 5 m and the length scale as the hub-to-hub distance of the hexacopter, which is equal to 0.6096 m (2 ft). The forward speed of the aircraft equal to 5 m/s and gross weight of 2 kg has been kept constant through the simulations. The data sets for aircraft states and controller commands are generated through a series of simulations for different turbulence levels (light, moderate and severe) for healthy aircraft and different fault types, such as various levels of degradation of front and side rotors. Degradation of rotors have been simulated by decreasing the output speed of the rotor by some ratio of that commanded by the controller. The rotor faults addressed in this work are degradation of front rotor (rotor 1), left-side rotor (rotor 2), and right-side rotor (rotor 6) (see Fig. 1). Next, similar data sets under different magnitude (1- 5 m/s) and directions of gusts for healthy flight under severe levels of turbulence have been generated (Ref. 20). The gusts follow a '1-cosine' shape with gradual increase, followed by a steady-state and gradual decrease (Ref. 21). The gusts have been further labelled as intermittent and longer gusts depending upon the time for which it lasts, the former being shorter than the latter. In real flight, the time and duration of gusts can be random in nature depending upon the region, altitude, and weather conditions. For a summary of the generated data sets, see Table 1. Note that the number of data sets in some categories are indicated as '$(\star + \dagger)$', where '$*$' stand for training sets and '$\dagger$' are the test data.

The time series (signals) of the hexacopter attitudes (aircraft states) and the control signals for the healthy state, flight affected by gusts, and different fault levels and types provide useful insight into the dynamics of the system.

General Workframe of Rotor Fault Detection and Identification

Let Z_o be signals that designate the aircraft under consideration in its healthy state, and Z_1, Z_2 and Z_6 the aircraft under fault of Rotor 1,2, and 6. Z_u designates the unknown (to be determined) state of the aircraft. Statistical learning methods explored in this study are based on discretized aircraft states signals $y[t]$ [1] and control signals $u[t]$ (for $t = 1, 2, \ldots, N$). Here, N denotes the number of samples and the conversion from discrete normalized time to analog time is based on $(t-1)T_s$, with T_s being the sampling period. The signals are represented by Z and subscript $(o, 1, 2, 6, u)$ is used to denote the corresponding state of the aircraft that produced the signals. To avoid numerical errors in the simulation, the signals are generated with a sampling frequency of 1000 Hz. Power Spectral Density of the signals show that the frequency range of interest is $0 - 50$ Hz. Consequently, they are downsampled to a sampling frequency, $F_s = 100$ Hz.

The signals generated from simulation can analyzed by parametric or non-parametric statistical methods and proper models are fitted and validated. Such models are trained for the cases Z_o, Z_1, Z_2, Z_6 in the baseline phase. Fault detection and identification is performed in the online inspection phase with the information extracted from the current unknown signals via the baseline models.

STATISTICAL PROCESS CONTROL CHARTS

Monitoring the statistical properties for aircraft control and response signals may lead to the early detection of abnormal conditions, and can also considered as a generic health monitoring function. When an aircraft experiences abnormal conditions, such as unexpected turbulence, gusts, or other hazardous events such as system faults, the mean and/or variance of the aircraft response and controller command signals are expected to change. Data from flight simulation of the multicopter under healthy condition can be used to establish proper and robust statistical thresholds under various environmental and flight conditions. To this end, standard statistical tools such as the $\bar{x}$ and S control charts (Ref. 22) may be employed to statistically monitor the sample mean and standard deviation values, respectively. As the statistical tools referring to quality assurance require serially uncorrelated observations (Ref. 23), an assumption certainly violated in the case of aircraft states and controller inputs, a prior action is necessary. Hence, the measured signals are modeled via simple Auto-Regressive time-series models, whose identification is described in detail in the following paragraph. This type of modeling is necessary to properly account for signal serial correlation. Following this, the statistical quality assurance tools are applied on the residuals(one-step-ahead prediction error) $e[t+1|t]]$ which satisfies the serial uncorrelatedness and normal distribution assumption.

[1] A functional argument in parentheses designates function of a real variable; for instance $x(t)$ is a function of analog time $t \in \mathbb{R}$. A functional argument in brackets designates function of an integer variable; for instance $x[t]$ is a function of normalized discrete time $(t = 1, 2, \ldots)$.

Table 1: Simulation Data

Aircraft state	Number of datasets			Signal Length (in s)
Healthy	Turbulence Levels			
	Severe	Moderate	Light	
	42+20	20	20	60
Gusts	Gust Wind Speed (in m/s)			
	5	2	1	
	64+80	80	80	20
	Degradation (in %)			
Rotor 1, 2, 6	20, 40, 60, 80	10, 30, 50, 70, 90	100	
Degradation	8+10	10	10	80
Sampling frequency: $f_s = 100$ Hz				

The general workflow for statistical process control charts in the baseline (offline) phase and inspection (online) phase is outlined in Figs. 3 and 4 respectively.

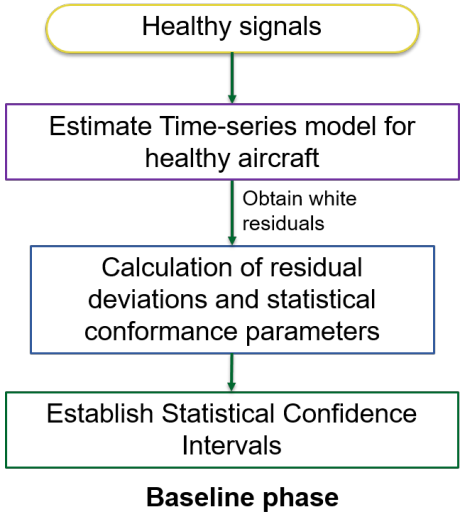

Figure 3: Statistical Process Control Charts

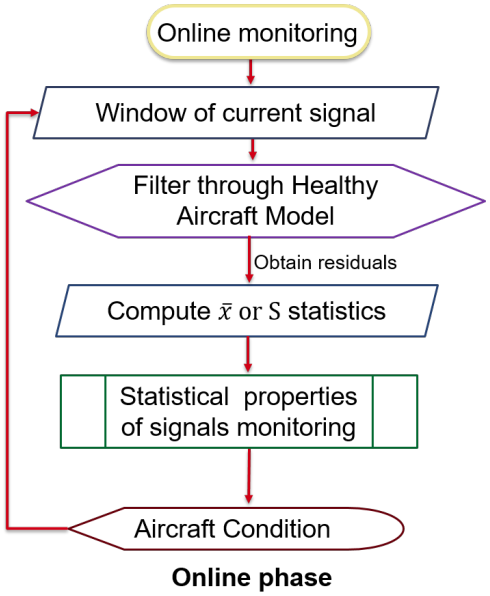

Figure 4: Statistical Process Control Charts

Scalar AR Identification Method

A single signal obtained from a healthy flight simulation is parametrized to form a scalar (univariate) AutoRegressive time series model (Ref. 24):.

$$y[t] + \sum_{i=1}^{na} a_i \cdot y[t-i] = e[t], \quad e[t] \sim \text{iid}\mathcal{N}(0, {\sigma_e}^2) \tag{3}$$

with a_i and na designating the AR parameters and model orders, respectively. 'iid' stands for identically independently distributed, and $\mathcal{N}(\cdot,\cdot)$ denotes a univariate normal distribution with the indicated mean and variance, respectively. In Eq. 3, $e[t]$ coincides with the one-step-ahead-prediction error and is also referred as the model residual sequence or innovations (Refs. 24, 25).

The identification of parametric time series models is comprised of two main tasks: parameter estimation and model order selection. The parameters for the AR model can been estimated by minimization of the Least Squares (LS) criterion (Refs. 25, 26), whereas the model order selection is achieved based on the examination of the Bayesian Information Criterion (BIC) (Refs. 25, 26) (Eq. 4) and Residual sum of Squares over Signal Sum of Squares Criterion (RSS/SSS) (Eq. 5). The former is a statistical criterion that penalizes model complexity (order, and hence the number of free parameters) as a counteraction to a decreasing model fit criterion. The latter determines the predictive capability of the model.

$$BIC = \ln \sigma_e^2 + (d \times \ln N)/N \tag{4}$$

$$RSS/SSS = \frac{\sum e^2[t]}{\sum y[t]^2} \qquad \forall \quad t = 0,1,...,N \qquad (5)$$

In Eq. 4, σ_e^2 is the variance of the residuals, d denotes the number of parameters to be estimated for the model and N denotes the number of samples used for estimation.

Statistical Monitoring

The residual signal $e[t]$ is obtained by filtering the current signal through the estimated model. Its standard deviation and mean denoted by $\sigma_e[t]$ and $\mu_e[t]$ respectively, are estimated via a non-overlapping sliding window of length m. The estimated sample standard deviation $\hat{\sigma}_e[t]$ and the sample mean $\hat{\mu}_e[t]$ become the charted values for the S and $\bar{x}$ charts respectively (Ref. 23). The average value of the standard deviation $\bar{S}$ is be calculated as $\bar{S} = mean[\sigma_e^i[t]]$. Similarly, $\bar{\bar{x}} = mean[\mu_e^i[t]]$.

The upper control limit (UCL), control limit(CL), and lower control limit(LCL) for the S-chart are defined as the following:

$$\text{UCL} = B_4\bar{S} \qquad \text{CL} = \bar{S} \qquad \text{LCL} = B_3\bar{S} \quad (6)$$

The corresponding $\bar{x}$-chart limits are defined as :

$$\text{UCL} = \bar{\bar{x}} + A_3\bar{S} \qquad \text{CL} = \bar{\bar{x}} \qquad \text{LCL} = \bar{\bar{x}} - A_3\bar{S} \quad (7)$$

The values of B_3, B_4 and A_3 are obtained from statistical tables or the following equations (Ref. 23) :

$$\begin{aligned} B_3 &= 1 - \frac{3}{c_4\sqrt{2(m-1)}} \\ B_4 &= 1 + \frac{3}{c_4\sqrt{2(m-1)}} \\ A_3 &= \frac{3}{c_4\sqrt{m}} \qquad \text{where } c_4 = \frac{4(m-1)}{4m-3} \end{aligned} \qquad (8)$$

The control charts constitute a means of monitoring the statistical properties of the signals. Abnormal deviations beyond the established upper and lower control limits serve as alarms for changes associated with various nominal events. It should be noted that the control limits are based on the normality assumption can often be successfully used, unless the population is extremely non-normal (Ref. 23, pg.203).

TIME-SERIES ASSISTED NEURAL NETWORKS

Machine learning techniques are being widely used in Fault Detection and Identification, to make decision on the current state of a dynamic system (Ref. 27). Classifiers such as Support Vector Machines and Neural Networks can accommodate noise and uncertainty in data with carefully chosen features and regularization parameters. This property of neural network makes it attractive for our application, where the focus is to develop a robust rotor FDI framework unaffected by disturbance due to gusts and noise due to turbulence encountered in real flight. The relationship between the control, and state signals for healthy flight without gusts can be modelled by time-series models. Next, the cross-correlation of control signals and state residuals obtained via the estimated model are extracted as explainable features that follow the dynamics of the hexacopter under different operating conditions.

The implementation of this method requires estimation of a statistical model for healthy aircraft and training a neural network to classify between healthy and faulty states in the baseline phase whose workflow is shown in Fig. 5. Online monitoring for fault detection and identification follows the flowchart shown in Fig. 6.

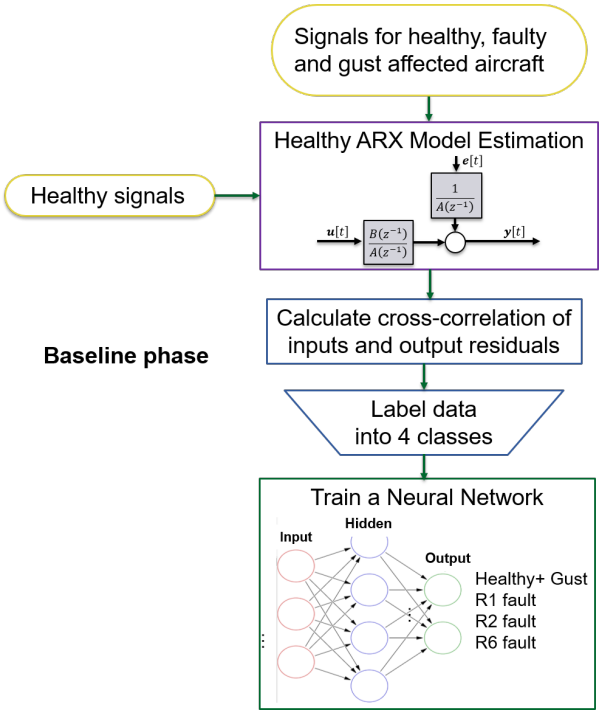

Figure 5: Time-Series Neural Networks: Baseline Phase

Vector ARX Model Identification for Healthy Aircraft

Vector AutoRegressive (VARX) models employ multi-dimensional signals, i.e. m-dimensional aircraft attitudes as the response and n-dimensional control signals as excitation, for input-output time series model-

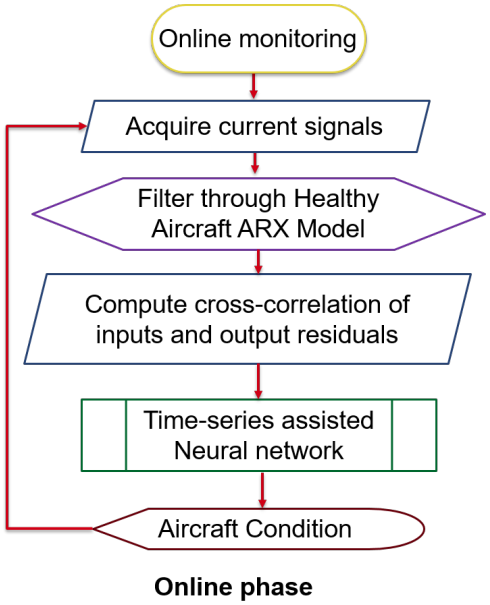

Figure 6: Time-Series Neural Networks: Online Phase

ing (Refs. 28, 29) given by:

$$\mathbf{y}[t]+\sum_{i=1}^{na}\mathbf{A}_i\cdot\mathbf{y}[t-i]=\sum_{i=0}^{nb}\mathbf{B}_i\cdot u[t-i-nk]+\mathbf{e}[t],\quad \text{with}$$
$$\mathbf{e}[t]\sim \text{iid}\,\mathcal{N}(\mathbf{0},\boldsymbol{\Sigma}),\quad \boldsymbol{\Sigma}=E\{\mathbf{e}[t]\cdot\mathbf{e}^T[t]\} \tag{9}$$

with $\mathbf{A}_i$ $(m\times m)$ designating the i-th AR matrix, $\mathbf{B}_i$ $(m\times n)$ designating the i-th X matrix, $\mathbf{e}[t]$ $(m\times 1)$ the model residual sequence characterized by the non-singular and generally non-diagonal covariance matrix $\boldsymbol{\Sigma}$, na the AR order, nb the X order, nk the delay in terms of lag between response and input signals and $E\{\cdot\}$ statistical expectation. Given the attitude signal measurements $y[t]$ $(t=1,2,\ldots,N)$, the estimation of the VARX parameter vector $\boldsymbol{\theta}$ comprising all AR and X matrix elements ($\boldsymbol{\theta}=\text{vec}([\mathbf{A}_1\quad \mathbf{A}_2\ldots\mathbf{A}_{na}\quad \mathbf{B}_0\quad \mathbf{B}_1\ldots\mathbf{B}_{nb}]$) and the residual covariance matrix $\boldsymbol{\Sigma}$ is accomplished via linear regression schemes based on minimization of the Ordinary Least Squares (OLS) or the Weighted Least Squares (WLS) criterion (Refs. 25, 26). The modeling procedure involves the successive fitting of VARX(na,nb,nk) models while sweeping through increasing AR and X orders, na and nb respectively and delay, nk, until an adequate model is achieved. The model order is chosen by similar fashion as AR model described in Section . But for vector models the equations for BIC and RSS are modified (Ref. 11) as follows :

$$BIC=\ln\left(trace(\boldsymbol{\Sigma})\right)+(d\times\ln N)/N \tag{10}$$

$$RSS/SSS=\sum_{i=1}^{m}\frac{\sum e_i^2}{\sum y_i[t]^2}\qquad\forall\quad t=0,1,...,N \tag{11}$$

Time-Series Assisted Neural Network

The VARX model for healthy aircraft is used to filter the aircraft signals (response and controls) and obtain output residuals. Important information about the dynamics of the aircraft is embedded in the output residuals and controller commands due to the incorporation of a feedback controller. To this effect, cross-correlation between the output residuals and inputs have been identified as a powerful feature to distinguish between different rotor faults and gust affected healthy flight.

The cross-correlation function between two signals $z(t)$ and $x(t)$, denoted by $\gamma_{zx}[\tau]$ is given by Eq. 12.

$$\gamma_{zx}[\tau]=E\{z[t]\cdot x[t+\tau]\} \tag{12}$$

where τ is the time lag in number of samples.

The cross-correlation function is fed to the input layer of a 2-layer neural network to classify 4 classes: healthy (without gusts and affected by gusts) and rotor 1, 2, and 6 degradation.

The input layer is denoted by $\mathbf{x}^T$ and the output layer is denoted by $\mathbf{h}(\mathbf{x})$ and is related by the following equation:

$$\mathbf{h}(\mathbf{x})=\theta\left(\mathbf{W_2}^T\left(\theta\left(\mathbf{W_1}^T\mathbf{x}\right)+\mathbf{B_1}\right)+\mathbf{B_2}\right) \tag{13}$$

where, $\theta(s)$ indicates the hyperbolic tangent activation function given by $\theta(s)=\dfrac{e^s-e^{-s}}{e^s+e^{-s}}$. The weight matrices and bias vectors for the two layers denoted by $\mathbf{W_1},\mathbf{W_2}$ and $\mathbf{B_1},\mathbf{B_2}$ are determined in the baseline training phase by backpropagation learning techniques to minimize classification error.

RESULTS AND DISCUSSION

Data Generation

Flight simulation for the hexacopter with a gross weight of 2 kg was performed at 5 m/s forward speed under severe, moderate and light turbulence levels according to the Dryden model. Figures 7 through 12 show control and attitude time histories of the hexacopter, for cases of healthy aircraft, flight under gusts and rotor degradation.

The aircraft response, namely roll, pitch, yaw, and altitude signals for flight under severe turbulence in absence of any rotor faults and gusts are shown in Fig. 7.

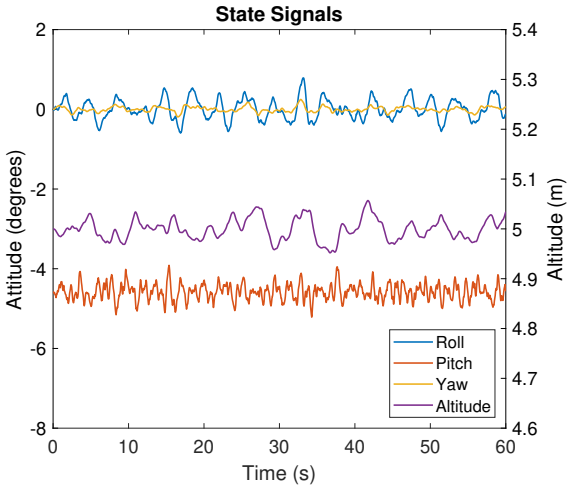

Figure 7: Attitudes state signals for healthy aircraft

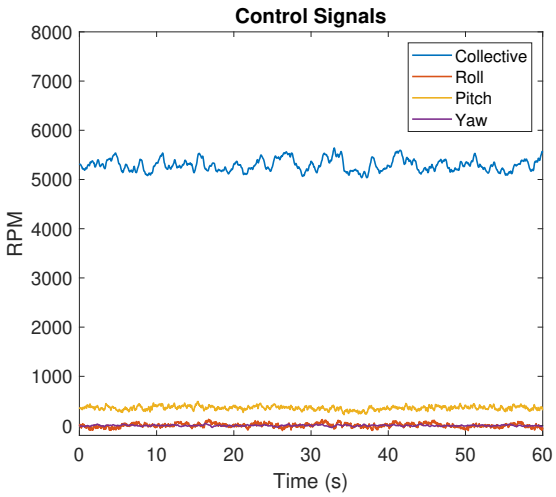

Figure 8: Control signals for healthy aircraft

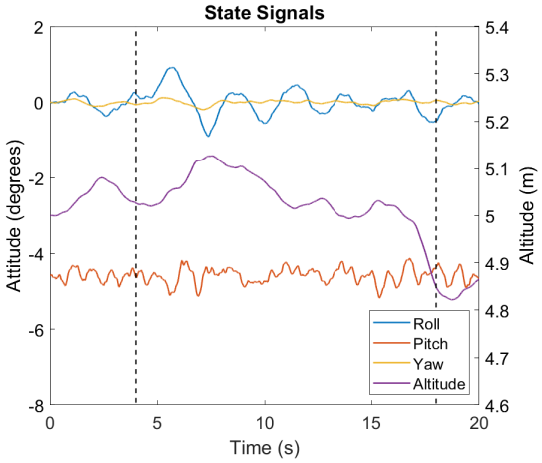

Figure 9: Attitudes state signals for flight affected by gusts of 5m/s

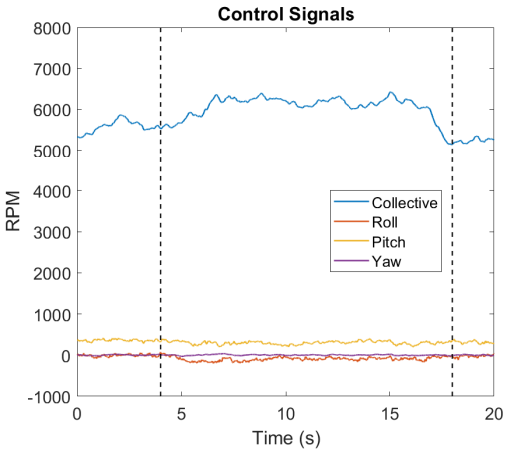

Figure 10: Control signals for flight affected by gusts of 5m/s

The corresponding linearly independent multicopter controls, namely collective, roll, pitch, and yaw control signals shown in Fig. 8 are derived from individual rotor speed commands via multirotor co-ordinate transform (Ref. 30). These signals are observed to be stationary, i.e have constant mean and standard deviation throughout the length of the flight.

Under gusts, the aircraft response deviates but is quickly compensated by the controller as seen in Fig. 9. On the other hand, the controller commands show a change in mean value for the duration of the gust (depicted by vertical black dashed lines) (Fig. 10). The magnitude, direction, and duration of gusts in real flight can be completely random in nature. The aircraft response and control signals for the gusts whose magnitude and direction which mimics rotor faults the most closely have been shown in this section. For the analysis, all possible directions and different magnitude of gusts have been considered.

In case of rotor faults, similar trends with aircraft response has been observed, where the initiation of fault is evident by the deviation from the nominal state, being followed by controller compensated state (Fig. 11). For the controller commands the change in statistical mean is observed after front rotor sees a degradation of 60%, throughout the rest of the flight duration (Fig. 12). Additional data for side rotor degradation and gusts have been shown in Appendix A (Figs. 18 through 21).

Statistical Process Control Charts

Statistical Process Control charts are used to monitor the changes that take place in a process by establishing con-

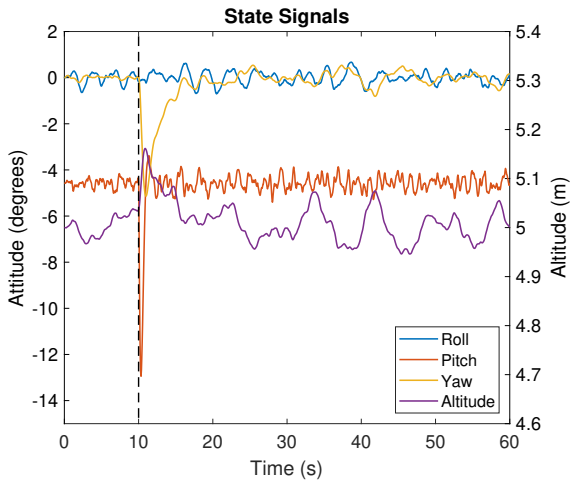

Figure 11: Attitudes state signals for 60% degradation of Rotor 1

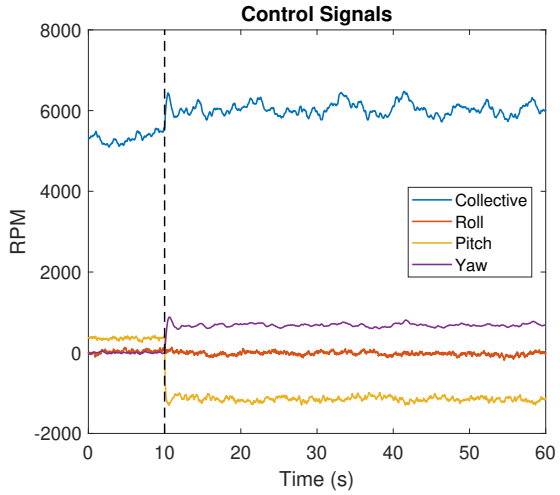

Figure 12: Control signals for 60% degradation of Rotor 1

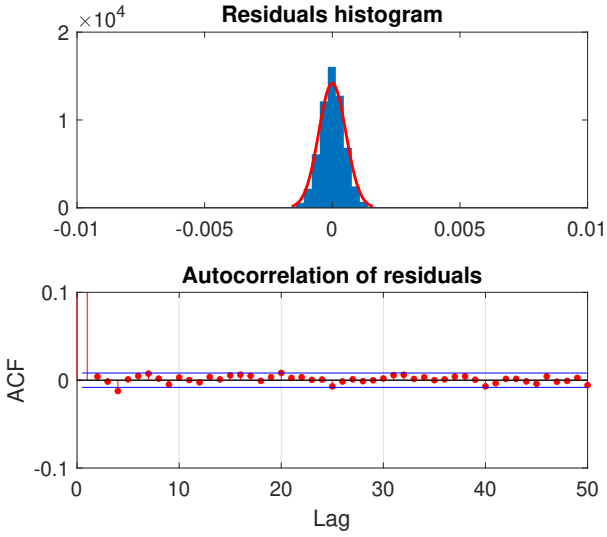

Figure 13: Residual Normality and Autocorrelation

trol limits which are violated in case of events beyond normal sampling variability.

Increase in the mean value of collective control in response to loss of thrust due to rotor degradation is highly indicative of a rotor fault if it persists for the entire length of flight. On the contrary, only certain gust directions will result in a change (increase/decrease of mean value) of the collective control command, but this lasts only for the duration of the gust. Therefore, monitoring the $\bar{x}$ statistics of the collective control signal can help distinguish between gusts and rotor faults. The signal is obtained from healthy aircraft flight simulation under severe turbulence, of length 60 s (N=60000 samples, F_s =1000 Hz) has been used to establish the statistical control limits. To this end, the collective control signal has been modeled by a simple AR(6) model, the model order chosen via BIC, to obtain white residuals that follow a normal distribution, as evident in Fig. 13. The UCL and LCL have been calculated by Eq. 6, where the length of non-overlapping window, $m = 1000$, and $\bar{\bar{x}}$ and $\bar{S}$ are the values of statistical expectation of the mean and variance of the non-overlapping windows of the residual sequence respectively. Here, the signal is divided into 60 segments, hence in online monitoring the test statistics are computed every 1 s.

Results for Statistical Process Control Charts Indicative results for $\bar{x}$ statistics monitoring under gusts of different duration and magnitude as well as different levels of front rotor (1) degradation is demonstrated in Figs. 14 and 15. It can be observed that due to gusts or faults the $\bar{x}$ statistics (shown by the x and +) violates the UCL and/or LCL given by red horizontal dashed lines, whereas for healthy flight without gusts (shown by the o) it always remains between the given limits.

Figure 14 shows that for the duration of the gusts the $\bar{x}$ statistics violate the UCL and LCL depending on the direction of the gusts, and the extent of violation depends on the magnitude of gusts. Intermittent gusts (shown by the +) of 2m/s are active for a 4 to 7 s window in every 10 s duration. Since this gust has a component coming from negative Z-direction (from below the aircraft), it causes the collective control to decrease and hence the LCL is violated for duration for which the gust is active. The longer gusts (shown by the x) have a magnitude of 5m/s, with a component in positive Z-direction and last for 4-18 s in every 20 s duration. Consequently, the $\bar{x}$ statistics exceed the UCL whenever the gust appears and goes back within the limits after it has passed.

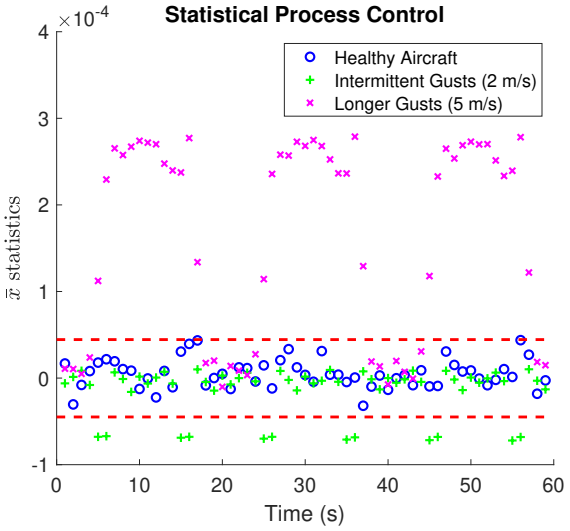

Figure 14: $\bar{\bar{x}}$ statistics monitoring on collective control signals under gusts

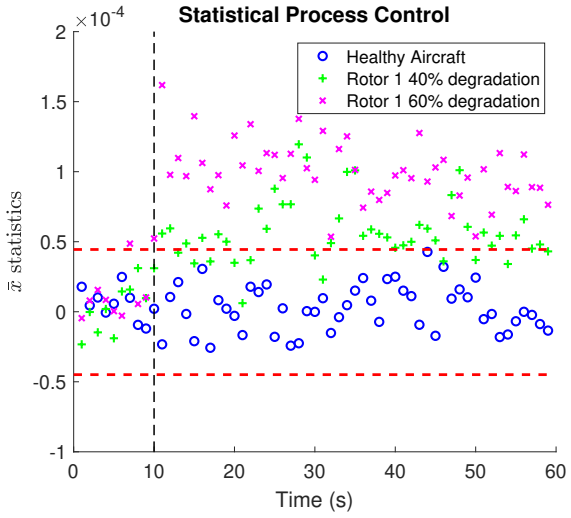

Figure 15: $\bar{\bar{x}}$ statistics monitoring on collective control signals under Rotor 1 degradation

In Fig. 15, the black vertical dashed line denotes the initiation of rotor 1 fault, after which the $\bar{x}$ statistics always crosses the UCL because the mean value of collective control signals always increases due to rotor degradation to compensate for loss of thrust. Though this method is very sensitive to even 20% rotor degradation, the test statistics continue to lie above the UCL only when the rotor losses speed of 60% or more of its nominal value. For less severe rotor degradation, the decision points show sporadic violation of UCL, in contrast to steady violation of UCL for more than 60% deterioration. Additional results for degradation of rotor 2 and 6 have been shown in Appendix B (Figs. 22 and 23).

Therefore, violation of the LCL is definitely an indication of gust because no rotor degradation would result in a decrease in mean rotor speed while maintaining the same flight condition. But for gusts resulting in updraft, monitoring control signals is not enough to distinguish them from faults. Though monitoring the $\bar{x}$ or S statistics of response signals may reveal more information, the fault identification by this method will become very complex or even impossible especially in the presence of more classes of faults. Also, it has been observed that S statistics do not have significant changes when applied to both control and response signals barring some initial change due to gust or fault initiation and thus has not been included in this study.

Time-series Assisted Neural Networks

Parametric Model Identification Vector (multivariate) parametric identification of the aircraft dynamics has been based on 40 s ($N = 4000$ samples at sampling frequency of 100 Hz) of aircraft attitude and control signals obtained from healthy aircraft flight at 5 m/s under severe turbulence. In the present case, the response comprises of the roll, pitch and yaw attitudes and the excitation is the multirotor controls, namely the collective, roll, pitch, and yaw controls. The model parameters and model order, A_i, B_i and na, nb, nk, respectively (Eq. 9), need to be estimated so that the model properly represents the dynamics of the system under healthy conditions. The modeling strategy consists of successive fitting of VAR(na, nb, nk) models until a suitable model with least amount of complexity (number of parameters) and best fit is selected.

Model order selection is based on a combination of Bayesian Information Criteria (BIC) (Eq. 4) and Residual sum of squares normalized by Signal sum of squares (RSS/SSS) criteria (Eq. 5). A model order of $na = 5, nb = 5, nk = 0$ yields the minimum BIC and this model is represented as VARX$(5,5,0)$. This order exhibits a very low RSS/SSS value of 2.4×10^{-3}% demonstrating accurate identification and excellent dynamics representation of the healthy aircraft at 5 m/s and under severe turbulence. The number of parameters estimated for the VARX$(5,5,0)$ model results in a Samples per Parameter (SPP) ratio of 38.09 ($\frac{N}{d}$), and the suggested value is more than 15 (Ref. 10).

The model was validated based on the fact that the model matching the current state of the system should generate output residual sequences which are uncorrelated with each other as well as the input signals. Consequently, a healthy aircraft signal has been generated from a different realization of severe turbulence. The cross-correlation function of the output residual sequences obtained from

driving the current signals from a healthy aircraft through the healthy model has been observed to be white with 95% confidence, as shown Fig. 16 (confidence intervals shown in blue). Next, the crosscorrelation function of input signals and output residuals have been presented in Fig. 17. It shows that the output residual sequences are uncorrelated with the past values of the inputs, i.e. for positive values of lag. For negative values of lag they are serially correlated, because the future values of inputs depend on the current output values due to the feedback controller in place.

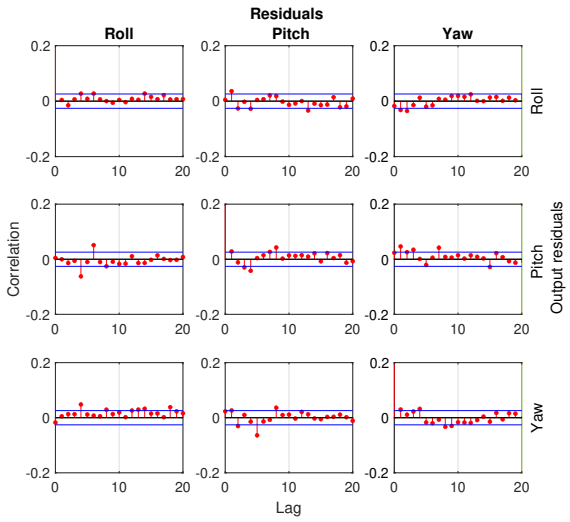

Figure 16: Residuals crosscorrelation

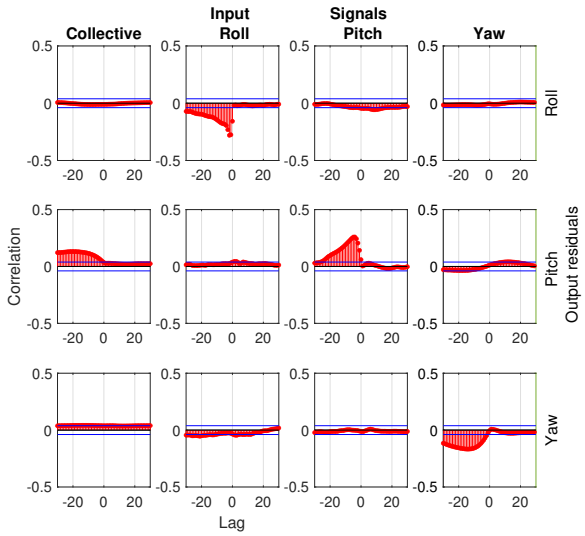

Figure 17: Input and residuals crosscorrelation

Training of Time-Series assisted Neural Network From Ref. 16, it has been observed that cross-correlation of output residuals, obtained via a statistical model of a healthy aircraft, have better capability to detect and identify rotor failures using simple neural network than signals only. Cross-correlation function serves as a "good" feature for fault classification. To this end, output residuals and input signals (controller commands) have been obtained from filtering the different healthy and faulty signals of 20s length through the healthy aircraft model. Next, the cross-correlation of these with each other up to positive and negative lag of 30 is fed through the first layer of the neural network. The first classification consists of healthy signals under severe turbulence with and without gusts (5 m/s with different direction and duration). The rotor 1, 2, and 6 fault classes have been trained with the respective defective rotor signals of 20, 40, 60, and 80% degradation. Therefore, this network, having output classes as healthy aircraft, rotor 1 fault, rotor 2 fault and rotor 6 fault, detects and identifies the rotor faults simultaneously. Note that the number of training data sets (See Table 1) should be balanced for the different classes to avoid classifier bias. The details of this neural network are given in Table 2.

Table 2: Time-Series assisted Neural network training

Input Type	Cross-correlation between output residuals and input signals (20 s)
Input Layer Size	1519
Training Function	Conjugate Gradient with Powell-Beale Restarts
Hidden Layer Size	10
Output Classes	4 (Healthy and Rotor 1,2 or 6 failures)
Cost Function	Cross-Entropy
Activation Function	Hyperbolic Tangent Function
Training termination	Validation
Performance	2.2×10^{-11}

Results for Time-Series assisted Neural Network Aircraft response and control signals obtained from current flight, with window length 5 s updated every 0.2 s, have been used for online monitoring by following the workflow depicted in Fig. 6. The neural network has been trained with information obtained from signals of length 20 s in the baseline phase for better tuning of weights and biases. In the online phase shorter signals of length 5 s have been utilized for faster FDI. To ascertain the generalization capability of the neural network, data from various unknown operating conditions have been applied which have not been used to train it. These conditions include moderate and lights levels of turbulence in healthy flight, gusts of 1 m/s and 2 m/s and rotor faults of 10, 30, 50, 70, 90, and 100% degradation has been applied. Note the neural network has only been trained with data

Table 3: Fault Detection and Identification results

Healthy aircraft under turbulence and gusts

Aircraft state	Accuracy of Classification (in %)		
Healthy	Turbulence Levels		
	Severe	Moderate	Light
	100	100	100
Gusts	Gust Wind Speed (in m/s)		
	5	2	1
	99.71	99.68	100

Faulty aircraft

Rotor Degradation	Accuracy of Classification (in %)								
	Degradation Levels (in %)								
	20	30	40	50	60	70	80	90	100
Rotor 1	100	100	100	100	100	99.82	99.60	99.82	99.86
Rotor 2	99.77	99.08	99.71	100	99.48	99.54	99.68	100	100
Rotor 6	99.59	100	100	99.97	100	100	99.91	99.42	99.80

sets of severe turbulence, 5 m/s gusts and 20, 40, 60, and 80 % rotor degradation. The performance of this neural network with test data sets is detailed in Table 3.

The computation time needed for classification in a single window is less than 0.07 s, therefore a window update interval of 0.2 s is reasonable. It has been observed that the false alarm rate is less than 0.32% even when the flight is affected by gusts. Also, the neural network is capable of classifying the intermediate rotor faults for which it has not been trained with fairly high accuracy. It should be noted that 10% rotor degradation has been classified as healthy in most cases because of negligible change in dynamics due to mild rotor speed reduction and that it extrapolates the training set which starts at 20% rotor degradation. Rotor degradation of 100% has been classified as the respective faulty rotor though it extrapolates the training set because of the considerable change in dynamics from the healthy state due to complete failure of the rotor. On average fault detection tales 0.7s from the initiation of fault, with a maximum of 2 s.

CONCLUSIONS

This paper introduces statistical time-series methods to detect and classify rotor faults in multicopters under turbulence and uncertainty while accurately rejecting disturbance due to gusts. Development of statistical time series models (response only and input-output) to represent healthy aircraft dynamics have been discussed followed by development of fault detection and identification methods assisted by information obtained from the model estimated from the healthy aircraft. The important conclusions from the study are summarized below.

- Statistical time series methods for rotor fault detection in multicopters achieve effective detection based on (i) ambient (white) excitation and aircraft state (*scalar* or *vector*) signals, (ii) statistical model building, and (iii) statistical decision making under uncertainty.
- Non-parametric methods like Statistical Process Control charts are simpler, but have similar sensitivity toward faults and gusts alike, which make them inapt for differentiating between the two.
- Statistical Process Control charts need investigation of multiple signals and complex decision trees to identify rotor faults while rejecting gusts.
- The knowledge of controller effort for different operating conditions like flight under gusts and rotor faults can be used along with the aircraft output to distinguish not only between healthy gust affected flight and faulty states but also classify the rotor faults.
- The cross-correlation function between input signals and output residuals obtained from a input-output statistical model for healthy aircraft serves as a powerful feature for a machine learning algorithm.
- With the right feature, which is the crosscorrelation function of signals obtained from various operating

conditions here, even a simple 2-layer neural network is capable of detecting and identifying rotor faults of even 20% degradation while disregarding aircraft response caused by gusts.

- In the online phase, the time-series assisted neural network has been shown to achieve fault detection and identification accuracy over 99% with signals having unknown operating conditions that are not used to train it.

- In the future, the modeling based fault detection identification methods will be explored to ascertain whether gusts change the healthy dynamics of the system at all. Also, a rational path forward will be to expand the scope of the Time-series assisted Neural Network to rotor degradation quantification.

AUTHOR CONTACT

Airin Dutta	duttaa5@rpi.edu
Michael McKay	mckaym2@rpi.edu
Fotis Kopsaftopolous	kopsaf@rpi.edu
Farhan Gandhi	fgandhi@rpi.edu

REFERENCES

1. Frangenberg, M., Stephan, J., and Fichter, W., "Fast Actuator Fault Detection and Reconfiguration for Multicopters," AIAA Guidance, Navigation, and Control Conference, January 2015. DOI: 10.2514/6.2015-1766

2. Heredia, G., and Ollera, A., "Sensor Fault Detection in Small Autonomous Helicopters using Observer/Kalman Filter Identification," IEEE International Conference on Mechatronics, Malaga, Spain, April 2009.

3. McKay, M., Niemiec, R., and Gandhi, F., "Post-Rotor-Failure-Performance of a Feedback Controller for a Hexacopter," American Helicopter Society 74th Annual Forum, Phoenix, AZ, May 2018.

4. Stepanyan, V., Krishnakumar, K., and Bencomo, A., "Identification and Reconfigurable Control of Impaired Multi-Rotor Drones," AIAA Science and Technology Forum and Exposition, January 2016.

5. Schneider, T., Ducard, G., Konrad, R., and Pascal, S., "Fault-tolerant Control Allocation for Multirotor Helicopters Using Parametric Programming," International Micro Air Vehicle Conference and Flight Competition, Braunschweig, Germany, 2012.

6. Saied, M., Lussier, B., Fantoni, I., Francis, C., Shraim, H., and Sanahuja, G., "Fault Diagnosis and Fault-Tolerant Control Strategy for Rotor Failure in an Octorotor," IEEE International Conference on Robotics and Automation (ICRA), Seattle, WA, May 2015.

7. Qi, X., Theillol, D., Qi, J., Zhang, Y., and Han, J., "A Literature Review on Fault Diagnosis Methods for Manned and Unmanned Helicopters," International Conference on Unmanned Aircraft Systems, May 2013.

8. Meskin, N., Khorasani, K., and Rabbath, C. A., "A Hybrid Fault Detection and Isolation Strategy for a Network of Unmanned Vehicles in Presence of Large Environmental Disturbances," *IEEE Transactions on Control Systems Technology*, Vol. 18, (6), January 2010, pp. 1422–1429.

9. Saied, M., Lussier, B., Fantoni, I., Francis, C., Shraim, H., and Sanahuja, G., "A Novel Robust Attitude Control for QuadrotorAircraft Subject to Actuator Faults and Wind Gusts," *IEEE/CAA Journal of Automatica Sinica*, Vol. 5, (1), January 2018, pp. 292–300.

10. Fassois, S., and Kopsaftopoulos, F., "Statistical Time Series Methods for Vibration Based Structural Health Monitoring," *New Trends in Structural Health Monitoring*, edited by W. Ostachowicz and J. Guemes, Springer, January 2013, pp. 209–264. DOI: 10.1007/978-3-7091-1390-5

11. Kopsaftopoulos, F. P., and Fassois, S. D., "Scalar and Vector Time Series Methods for Vibration Based Damage Diagnosis in a Scale Aircraft Skeleton Structure," *Journal of Theoretical and Applied Mechanics*, Vol. 49, (4), 2011, pp. 727–756.

12. Samara, P. A., Fouskitakis, G. N., Sakellariou, J. S., and Fassois, S. D., "A Statistical Method for the Detection of Sensor Abrupt Faults in Aircraft Control Systems," *IEEE Transactions on Control Systems Technology*, Vol. 16, (4), July 2008, pp. 789–798. DOI: 10.1109/TCST.2007.903109

13. Kopsaftopoulos, F. P., and Fassois, S. D., "A vibration model residual-based sequential probability ratio test framework for structural health monitoring," *Structural Health Monitoring*, Vol. 14, (4), 2015, pp. 359–381.

14. Dimogianopoulos, D. G., Hios, J. D., and Fassois, S. D., "FDI for Aircraft Systems Using Stochastic Pooled-NARMAX Representations: Design and

Assessment," *IEEE Transactions on Control Systems Technology*, Vol. 17, (6), nov 2009, pp. 1385–1397.

15. Dutta, A., McKay, M., Kopsaftopoulos, F., and Gandhi, F., "Rotor Fault Detection and Identification on a Hexacopter Based on Statistical Time Series Methods," Vertical Flight Society 75th Annual Forum, Philadelphia, PA, May 2019.

16. Dutta, A., McKay, M., Kopsaftopoulos, F., and Gandhi, F., "Fault Detection and Identification for Multirotor Aircraft by Data-Driven and Statistical Learning Methods," Electric Aircraft Technologies Symposium (EATS), Indianapolis, IN, August 2019.

17. Dutta, A., McKay, M., Kopsaftopoulos, F., and Gandhi, F., "Statistical Time Series Methods for Multicopter Fault Detection and Identification," Vertical Flight Society International Powered Lift Conference, San Jose, CA, Jan 2020.

18. Peters, D., and He, C., "A Finite-State Induced Flow Model for Rotors in Hover and Forward Flight," American Helicopter Society 43rd Annual Forum, St. Louis, MO, May 1987.

19. Hakim, T. M. I., and Arifianto, O., "Implementation of Dryden Continuous Turbulence Model into Simulink for LSA-02 Flight Test Simulation," Journal of Physics: Conference Series 1005(2018) 012017, August 2018.

20. Palomaki, R. T., Rose, N. T., van den Bossche, M., Sherman, T. J., and Wekker, S. F. J. D., "Wind Estimation in the Lower Atmosphere Using Multirotor Aircraft," *Journal of Atmospheric and Oceanic Technology*, May 2017. DOI: 10.1175/JTECH-D-16-0177.1

21. Wang, B. H., Wang, D. B., Ali, Z. A., Ting, B. T., and Wang, H., "An Overview of Various Kinds of Wind Effects on Unmanned Aerial Vehicle," *Journal of Measurement and Control*, Vol. 52, (7-8), September 2019, pp. 731–739. DOI: 10.1177/0020294019847688

22. Sotiriou, D., Kopsaftopoulos, F., and Fassois, S., "An Adaptive Time-Series Probabilistic Framework for 4-D Trajectory Conformance Monitoring," *IEEE Transactions on Intelligent Transportation Systems*, Vol. 17, (6), June 2016, pp. 1606 – 1616. DOI: 10.1109/TITS.2015.2511024

23. Montgomery, D. C., *Introduction to statistical quality control*, John Wiley & Sons Inc., 6th edition, 2009.

24. Box, G. E. P., Jenkins, G. M., and Reinsel, G. C., *Time Series Analysis: Forecasting & Control*, Prentice Hall: Englewood Cliffs, NJ, third edition, 1994.

25. Ljung, L., *System Identification: Theory for the User*, Prentice–Hall, second edition, 1999.

26. Fassois, S. D., "Parametric identification of vibrating structures," *Encyclopedia of Vibration*, edited by S. Braun, D. Ewins, and S. Rao, Academic Press, 2001, pp. 673–685.

27. Ganguli, R., Chopra, I., and Haas, D. J., "Helicopter Rotor System Fault Detection Using Physics-Based Model and Neural Networks," *AIAA Journal*, Vol. 36, (6), May 1998, pp. 1078–1086.

28. Söderström, T., and Stoica, P., *System Identification*, Prentice–Hall, 1989.

29. Lütkepohl, H., *New Introduction to Multiple Time Series Analysis*, Springer-Verlag Berlin, 2005.

30. Niemiec, R., and Gandhi, F., "Multi-Rotor Coordinate Transforms for Orthogonal Primary and Redundant Control Modes for Regular Hexacopters and Octocopters," 42nd Annual European Rotorcraft Forum, Lille, France, September 2016.

APPENDIX

A. Data Generation

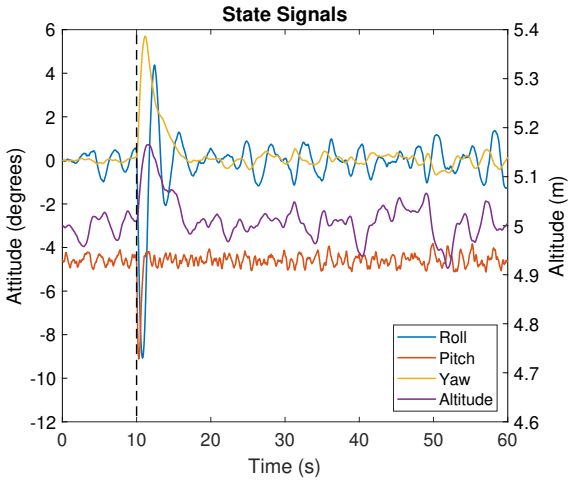

Figure 18: Attitudes state signals for 60% degradation of Rotor 2

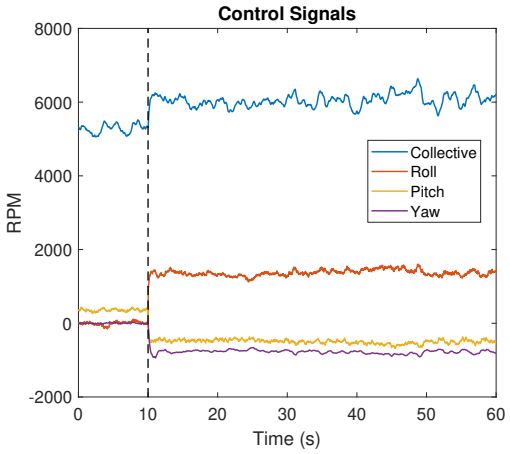

Figure 19: Control signals for 60% degradation of Rotor 2

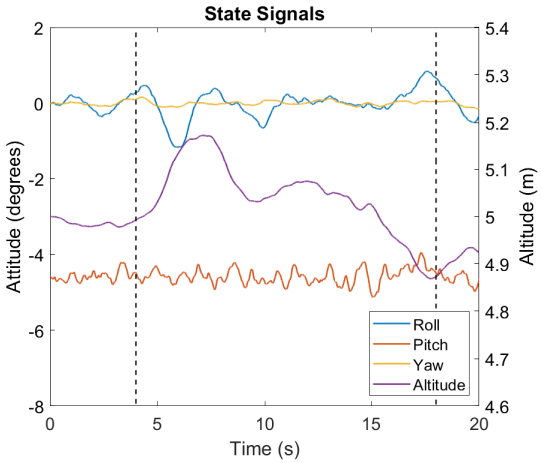

Figure 20: Attitudes state signals for flight affected by gusts of 5m/s

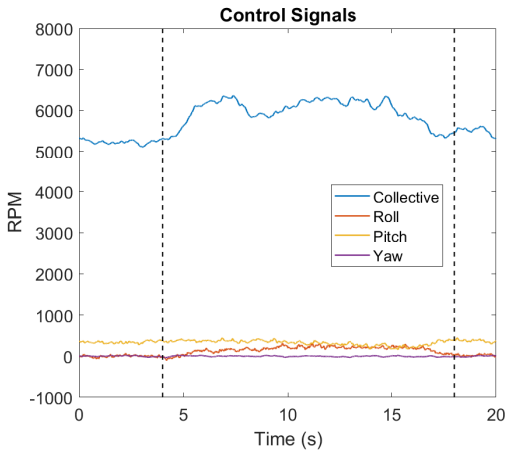

Figure 21: Control signals for flight affected by gusts of 5m/s

B. Statistical Process Control Chart

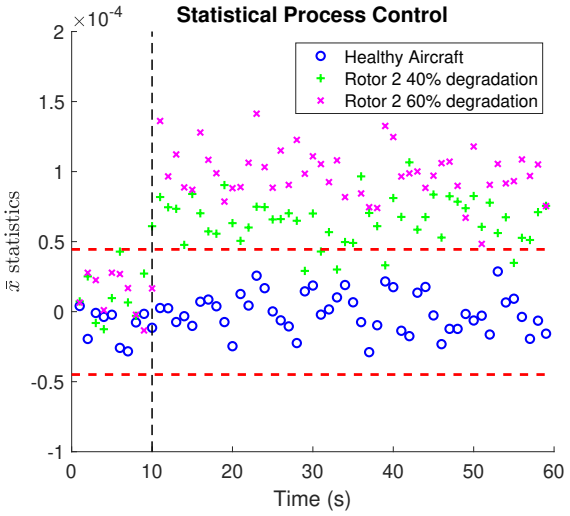

Figure 22: $\bar{\bar{x}}$ statistics monitoring on collective control signals under Rotor 2 degradation

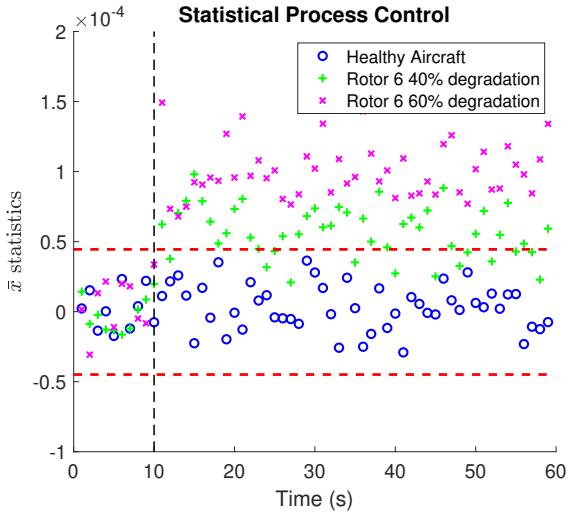

Figure 23: $\bar{\bar{x}}$ statistics monitoring on collective control signals under Rotor 6 degradation